ExoMol line lists – LXV. Mid-Infrared rovibronic spectroscopy of isotopologues of NiH

Kirill Batrakov, Sergei N Yurchenko, Alec Owens, Jonathan Tennyson, Alexander O. Mitrushchenkov, Amanda J. Ross, Patrick Crozet, Asen Pashov

ExoMol line lists – LXV. Mid-Infrared rovibronic spectroscopy of isotopologues of NiH

Kirill Batrakov,[1] Sergei N. Yurchenko,[1] Alec Owens,[1] Jonathan Tennyson,[1]★
Alexander Mitrushchenkov,[2] Amanda J. Ross,[3] Patrick Crozet,[3] Asen Pashov[4]

[1] *Department of Physics and Astronomy, University College London, Gower Street, WC1E 6BT London, UK*
[2] *MSME, Université Gustave Eiffel, CNRS UMR 8208, Univ Paris Est Creteil, F-77474 Marne-la- Vallée, France*
[3] *University of Lyon, Université Claude Bernard Lyon 1 & CNRS, Institute Lumiére Matiére UMR 5309, F-69622, Villeurbanne, France*
[4] *Faculty of Physics, Sofia University, 5 James Bourchier Boulevard, 1164 Sofia, Bulgaria*

5 December 2024

ABSTRACT

New line lists for four isotopologues of nickel monohydride, ^{58}NiH, ^{60}NiH, ^{62}NiH, and ^{58}NiD are presented covering the wavenumber range < 10000 cm^{-1} ($\lambda > 1$ μm), J up to 37.5 for transitions within and between the three lowest-lying electronic states, $X\,^2\Delta$, $W\,^2\Pi$, and $V\,^2\Sigma^+$. The line lists are applicable for temperatures up to 5000 K. The line lists calculations are based on a recent empirical NiH spectroscopic model [Havalyova et al. *J. Quant. Spectrosc. Radiat. Transf.*, **272**, 107800, (2021)] which is adapted for the variational nuclear-motion code Duo. The model consists of potential energy curves, spin-orbit coupling curves, electronic angular momentum curves, spin-rotation coupling curves, Λ-doubling correction curve for $^2\Pi$ states and Born-Oppenheimer breakdown (BOB) rotational correction curves. New *ab initio* dipole moment curves, scaled to match the experimental dipole moment of the ground state, are used to compute Einstein A coefficients. The BYOT line lists are included in the ExoMol database at www.exomol.com.

Key words: line: profiles - molecular data - exoplanets - stars: atmospheres - stars: low-mass

1 INTRODUCTION

Ni has a cosmic abundance similar to that of chromium or calcium, so the nickel hydride (NiH) molecule could reasonably be considered a target species for astrophysical observations. Its spectrum in the visible region happens to be overlapped by strong bands of TiO, possibly explaining why it has not joined CrH and FeH in the list of well-known absorbers in stellar atmospheres, but strong rotation-vibration and ro-vibronic systems are to be expected further to the infrared. This paper focuses on transitions occurring within the three low-lying 'supermultiplet' states of NiH, characterized by large permanent dipole moments close to their equilibrium internuclear distances. Few of these transitions have been observed directly, but many can be predicted from term energies extracted from potential energy curves and coupling functions derived from the analysis of optical data.

We have adjusted the model proposed by Havalyova et al. (2021) to suit the framework of program Duo (Yurchenko et al. 2016), and have created an NiH line list as part of the ongoing ExoMol project (Tennyson & Yurchenko 2012; Tennyson et al. 2024). This entailed computation of permanent and transition dipole moments, as well energy levels, and then compilation of an optimized data base where experimentally-derived energies replace calculated quantities wherever possible. These line lists should aid observation and assignments of NiH in cool stars and elsewhere.

Brown and Evenson and their co-workers (Beaton et al. 1988; Nelis et al. 1991; Brown et al. 1993) were amongst the first to provide spectroscopic data on NiH with the specific purpose of supporting the search for NiH in astrophysical media. They used laser magnetic resonance to measure pure rotation in the far IR. Around the same time, the Urban group explored transitions within the 2D ground state manifold, and between the $X\,^2\Delta$ and $W\,^2\Pi$ states of NiH and NiD (Lipus et al. 1989, 1993; Bachem et al. 1991), establishing energy levels more accurately than the earlier emission studies from a hollow cathode lamp (Scullman et al. 1982) or absorption (Kadavathu et al. 1987) in a King furnace had done. Steimle et al. (1990) measured Λ-doubling splittings in microwave spectra of the ground state of ^{58}NiH and ^{60}NiH, noting the influence of mixing between states, since 'normal' Δ states were not then expected to show significant Λ-doubling. In later years, laser excitation and fluorescence in the optical domain became increasingly important in the study of NiH, with work notably from the Field group at MIT providing a great deal of insight into the electronic structure of NiH. Hill & Field (1990) observed the $W\,^2\Pi$ and $V\,^2\Sigma^+$ states through laser-induced fluorescence, giving further details in Kadavathu et al. (1990). Their supermultiplet model (Gray et al. 1990) was published shortly afterwards, demonstrating that atomic parameters can account for much of the molecular structure in these three low-lying states, including effective Landé factors determined from Zeeman spectroscopy (Li & Field 1989; McCarthy et al. 1997). Intracavity laser absorption spectroscopy approach was used by O'Brien & O'Brien (2005); Shaji et al. (2008, 2009) to study $B\,^2\Delta - X\,^2\Delta$ transitions for the four

★ The corresponding author: j.tennyson@ucl.ac.uk

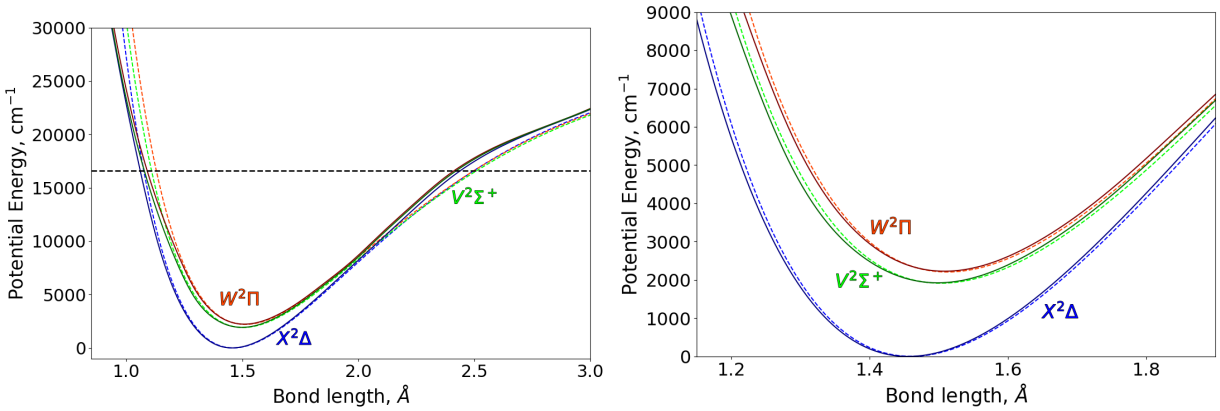

Figure 1. Comparison of our refined PECs of NiH to those from Havalyova et al. (2021). Darker shades of colours correspond to the curves from Havalyova et al. (2021). Lighter shades of colours correspond to our refined curves. The horizontal dashed line shows where the first of higher-lying electronic states with allowed transitions start according to Zou & Liu (2007). The right display zooms in on the spectroscopically important region.

dominant nickel isotopes. All these studies facilitated work from the Lyon group, who recorded isotopically selective dispersed fluorescence spectra on a Fourier transform instrument, both for NiH (Ross et al. 2012; Vallon et al. 2009) and NiD (Abbasi et al. 2018; Ross et al. 2019), using a sputtering source operating around 450 K.

Theoretical studies of NiH started with Guse et al. (1977) who made an early attempt to describe the potential energy curves (PECs) of NiH. However, this study was not successful in describing the complex electronic structure of the molecule, as they did not show that PECs corresponding to the three lowest electronic states $X\,^2\Delta$, $W\,^2\Pi$, $V\,^2\Sigma^+$ have similar shapes and lie close to each other. Later, Bagus & Bjorkman (1981) identified this behaviour which was confirmed by Blomberg et al. (1982). Further development of theoretical methods for calculations of NiH PECs and energy levels were carried out by Walch & Bauschlicher (1983), Ruette et al. (1984). A more precise description of relativistic effects in the molecule was obtained by Marian et al. (1989). Due to the similarity of PECs of the three lowest electronic states, a supermultiplet approach, which does the fitting of energy levels for all electronic states simultaneously, was proposed in Gray et al. (1991). Further theoretical work was carried out by Pouamerigo et al. (1994) with a focus on chemical bonds of NiH, by Diaconu et al. (2004) with a focus on the application of hybrid density functional theory and by Goel & Masunov (2008) who compared different techniques on 3d transition metal hydrides. Zou & Liu (2007) presented probably one of the most detailed *ab initio* studies on NiH PECs, as they considered several higher-lying electronic states as well.

Studies on the NiH dipole moments are less extensive. The first experimental study of electric dipole moment properties of NiH was carried out by Gray et al. (1985) who measured the ground state dipole moment, 2.4 ± 0.1 Debye. Later, Chen & Steimle (2008) confirmed and refined the previous result to 2.44 ± 0.02 Debye. Different theoretical methods were used to calculate dipole moments by Walch et al. (1985), who computed values in the range 1.74 – 3.98 Debye using different techniques, and Bauschlicher et al. (1990), who computed values in the range 1.544 – 3.310 Debye using different techniques. Thus the agreement between experiments and theoretical techniques remain uncertain.

Havalyova et al. (2021) presented a spectroscopic model for low-lying electronic states of NiH. This model accurately predicts the energy term values for the three lowest-lying electronic states of ^{58}NiH, ^{60}NiH, ^{62}NiH isotopologues. Havalyova et al. (2021) fitted cubic spline pointwise (PECs and relevant couplings) curves to experimentally derived energies of NiH from a series of spectroscopic studies by Steimle et al. (1990); Lipus et al. (1992); Vallon et al. (2009); Ross et al. (2012); Abbasi et al. (2018). However, Havalyova et al. (2021) made no mention of transition intensities. Abbasi et al. (2018) presents the most detailed combined experimental-theoretical study of the ^{58}NiD isotopologue up to date, giving the model in terms of Dunham-type parameters, again with no information on the intensities. Since that paper was published, more low-Ω levels of NiD have been reported by Ross et al. (2019), motivating further analysis.

In this work, we provide comprehensive infrared ($\lambda > 1$ μm) line lists for four isotopologues of nickel hydride (^{58}NiH, ^{60}NiH, ^{62}NiH, and ^{58}NiD) in their three lowest electronic states ($X\,^2\Delta$, $W\,^2\Pi$, $V\,^2\Sigma^+$), containing transition frequencies and Einstein A coefficients, as well as data on individual energy levels, including their lifetimes. To this end, we combine the spectroscopic model from Havalyova et al. (2021) with a new set of *ab initio* dipole moment curves (DMCs). The line lists were computed using the Duo software (Yurchenko et al. 2016).[1] The potential energy and coupling curves of Havalyova et al. (2021) are refitted to make them compatible with Duo, while the *ab initio* DMCs are scaled to the experiment (Chen & Steimle 2008). We believe that these line lists are robust enough to be used in astrophysical observations of spectra and the detection of NiH in astrophysical media.

2 SPECTROSCOPIC MODEL

2.1 Energy calculations

We used the Duo (Yurchenko et al. 2016) program to solve the coupled system of Schrödinger equations. The grid of 301 points with the bond length range 0.75 – 4 Å and a basis set of $v_{max} = 40$ were used in conjunction with the Sinc DVR method. The details of the Duo methodology can be found in Yurchenko et al. (2016).

As a starting point in our calculations we used the empirical spectroscopic model of NiH recently produced by Havalyova et al. (2021). Their model consists of three PECs, all relevant spin-orbit curves (SOCs), electronic angular momentum curves (EAMCs, also known

[1] Duo is a Fortran 2003 program freely available from www.github.org/exomol

as L-uncoupling curves), spin-rotation curves (SRCs) as well as Born-Oppenheimer breakdown (BOB) curves. The curves are given in a pointwise grid representation in conjunction with cubic spline interpolation. Due to functional representations of the off-diagonal couplings between Duo and the computational method used by Havalyova et al. (2021), we could not port their model directly into Duo one-to-one. For example, Duo uses a different representation for the BOB and Λ-doubling effects. Hence, we could not reproduce their results with Duo with sufficiently good accuracy and decided to further transform their model by refitting to the same set of the experimental data, covering experimentally derived energies of ^{58}NiH, ^{60}NiH and ^{62}NiH in their three lowest electronic states $X\,^2\Delta$, $W\,^2\Pi$, $V\,^2\Sigma^+$ as reported in Havalyova et al. (2021). We also include the ^{58}NiD isotopologue into the current work and build and a similar empirical model for which experimental energy term values from Abbasi et al. (2018) were used.

As far as the intensity calculations are concerned, we have computed electric (transition) dipole moment curves of NiH between the electronic states $X\,^2\Delta$, $W\,^2\Pi$, $V\,^2\Sigma^+$ *ab initio* as discussed below.

2.2 Analytical Description of the Spectroscopic Model of NiH

In order to make the spectroscopic model by Havalyova et al. (2021) compatible with Duo, we had to convert their curves from their pointwise grid representation to an analytic representation used in Duo. In the following, we introduce the analytic representation of the curves used in the refinement of the spectroscopic model by Abbasi et al. (2018) and discuss the effect of this modifications.

An Extended Morse Oscillator (EMO) function (Lee et al. 1999) was used to represent PECs for all electronic states:

$$V(r) = V_\mathrm{e} + (A_\mathrm{e} - V_\mathrm{e})\left[1 - \exp\left(-\sum_{k=0}^{N} B_k \xi_p^k (r - r_\mathrm{e})\right)\right], \quad (1)$$

where r_e is an equilibrium distance, A_e is a dissociation asymptote, $A_\mathrm{e} - V_\mathrm{e}$ is a dissociation energy, ξ_p is the Šurkus variable given by

$$\xi_p = \frac{r^p - r_\mathrm{e}^p}{r^p + r_\mathrm{e}^p}. \quad (2)$$

where p the exponent is chosen as part of the fit.

Figure 1 shows the original PECs by Havalyova et al. (2021) and compares them to our refined PECs. The horizontal dashed line at 16500 cm^{-1} indicates the region of the strong spectroscopic presence of NiH in the visible region due to the next family of the doublet electronic states of NiH, see the *ab initio* study by Zou & Liu (2007). The differences caused by the fits are small, especially in the spectroscopically relevant region below 10000 cm^{-1}. This is reassuring as essentially we attempt to reconstruct the same spectroscopic model and the differences should be mainly due to different responses of our models to the ambiguities from the limited amount of the underlying experimental information. Figure 2 provides a similar comparison between the SOCs, obtained in this work and from Havalyova et al. (2021). These differences, as well as analogous difference between other couplings from these two studies, is manifestation of the strong correlation between different components defining our models and thus is reflection of the complexity of the system.

The following function was initially used to describe all the coupling and correction curves:

$$F(r) = \sum_{k=0}^{N} B_k z^k (1 - \xi_p) + \xi_p B_\infty \quad (3)$$

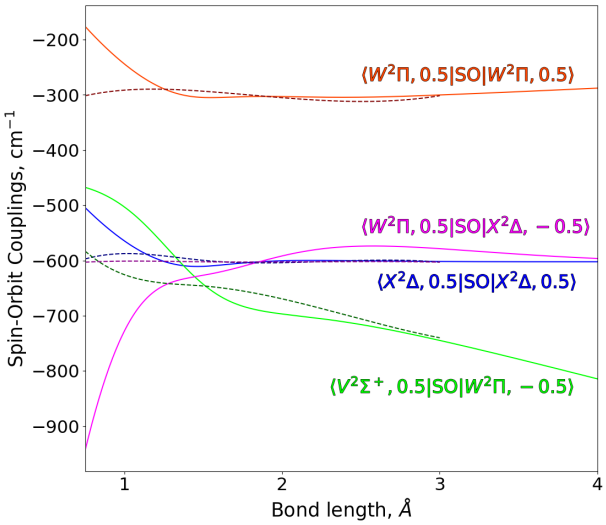

Figure 2. SOC obtained in this work (solid lines and lighter shades of colours) and by Havalyova et al. (2021) (dashed lines and darker shades of colours). Captions on the figure show what are the electronic states involved and corresponding values of Σ, the projection of the spin of electrons on the molecular axis.

where z is a coordinate damped at large r as given by

$$z = (r - r_\mathrm{ref}) \exp\left(-\beta_2 (r - r_\mathrm{ref})^2 - \beta_4 (r - r_\mathrm{ref})^4\right), \quad (4)$$

see Prajapat et al. (2017) and Yurchenko et al. (2018a) for more details. Here r_ref is a reference position which equals r_e by default, β_2 and β_4 are damping parameters, B_∞ is a long-range asymptote, usually fixed to 0 or 1. The functional formed used do not provide any control over short values of r and are theretofore prone to divergence as a result of the refinement due to the lack of constraints from experimental data at high very energies specific for the short distances.

We therefore modified Eq. (4) by incorporating a short-distance damping function based on a form proposed by Douketis et al. (1982) as given by

$$F(r) = D^\mathrm{DS}(r) \sum_{k=0}^{N} B_k z^k (1 - \xi_p) + \xi_p B_\infty, \quad (5)$$

which differs from the Eq. (3) by an additional damping term

$$D^\mathrm{DS}(r) = \left[1 - \exp\left(-br - cr^2\right)\right]. \quad (6)$$

Here, b, c, and s are short-range damping parameters, see Douketis et al. (1982); Robert J. Le Roy & Li (2011); Le Roy (2017) for more details. This damped formula was used for one SOC, $\langle W\,^2\Pi|\mathrm{SO}|X\,^2\Delta\rangle$, all spin-rotation couplings, and all BOB-rotation corrections. Other couplings and dipole moment curves were modelled using Eq. (3). Figure 3 shows the final curves for the ^{58}NiH isotopologue. We used the same curves for ^{60}NiH and ^{62}NiH with the exception of the BOB-rotation correction, which were refitted due to the changed mass. A similar approach was used for the ^{58}NiD isotopologue, but the quality of the fit decreased by two orders of magnitude, mainly due to more limited experimental coverage. Thus, for ^{58}NiD we also had to refit diagonal spin-orbit coupling curves ($\langle X\,^2\Delta\,|\mathrm{SO}|X\,^2\Delta\rangle$ and $\langle W\,^2\Pi|\mathrm{SO}|W\,^2\Pi\rangle$) and add diabatic diagonal couplings for $X\,^2\Delta$ and $W\,^2\Pi$ states as a correction to their PECs (it turned out to be more efficient than varying PECs themselves). The latter were modelled

using Eq. (3). The bottom-right display of Fig. 3 shows these diabatic coupling curves of ^{58}NiD.

The root mean square (rms) deviation of energy terms values computed using our model from the experimental values were: 0.036 cm^{-1} for ^{58}NiH, 0.029 cm^{-1} for ^{60}NiH, 0.017 cm^{-1} for ^{62}NiH, and 0.061 cm^{-1} for ^{58}NiD. ^{60}NiH and ^{62}NiH had fewer experimental term values (J_{max} = 12.5 and 9.5, respectively) than ^{58}NiH (J_{max} = 16.5). For ^{58}NiD, J_{max} = 17.5. It is important to note that the model presented by Havalyova et al. (2021) is more accurate than our work, as they got rms deviations in the range of 0.011 – 0.015 cm^{-1}, which can be attributed to a more efficient fitting procedure used by Havalyova et al. (2021).

2.3 Dipole Moments

We used the MCSCF/aug-cc-pVTZ-DK level of theory to compute (transition) dipole moment curves between the three lowest electronic states of NiH using the MOLPRO software (Werner et al. 2012). The diagonal ones are shown in Fig. 4. The non-diagonal (transition) dipoles were two orders of magnitude smaller than the diagonal ones (< 0.09 Debye).

The study by Chen & Steimle (2008) measured the permanent dipole moment for the ground $X\,^2\Delta$ state using the optical Stark effect, for which they obtained 2.44 Debye. This value can be compared to the value of the permanent moment of $X\,^2\Delta$ state of 3.13 D at $r = r_e$ and to the vibrationally averaged value (v = 0) of 3.16 D computed with Duo. Increasing the *ab initio* level of theory to significantly more expensive MRCI/aug-cc-pVTZ-DK only reduced it to 3.1 D, i.e had a negligible effect. We therefore decided to empirically adjust the DMC of $X\,^2\Delta$ by scaling our MCSCF curve by the factor of the ratio of the experiment over theory (2.44/3.16 = 0.77). Unfortunately, there is no experimental information on other two diagonal dipole moments, $W\,^2\Pi$ and $V\,^2\Sigma^+$. Considering that all three *ab initio* curves appear to closely follow each other, see Fig. 4, we decided to apply the same scaling of 0.77 also to these two curves. The non-diagonal (transitional) dipoles were not scaled, as their shapes do not follow the diagonal curves. Dipole moment curves were not changed between different isotopologues.

The three diagonal DMCs were then modelled using the analytic description of Eq. (3). This was important to reduce numerical noise typical for high vibrational overtones leading to the so-called "overtone plateaus" (Medvedev et al. 2016). As part of this treatment, we also applied a threshold to vibrational transitional moments of 10^{-8} Debye.

Spectroscopic models for all isotopologues can be found in the supplementary data in the form of input files for Duo.

3 LINE LIST

Line lists for four isotopologues of NiH, ^{58}NiH, ^{60}NiH, ^{62}NiH, and ^{58}NiD were generated using the empirical spectroscopic model constructed and the scaled *ab initio* MCSCF DMCs for $X\,^2\Delta$, $W\,^2\Pi$, and $V\,^2\Sigma^+$ states. The line lists BYOT cover the wavenumber range up to 10000 cm^{-1} with rotation excitations up to J = 56.5 (NiH) and J = 78.5 (NiD). We used the lower state cutoff of 20000 cm^{-1} aiming at the completeness at high temperatures even at lower frequencies. Table 1 shows the number of states and transitions computed for each isotopologue.

The line lists are provided in the standard ExoMol format (Tennyson et al. 2013, 2020) with States and Trans files. Tables 2 and 3 show examples of extracts from these files for ^{58}NiH. The States file contains the following information for each energy term: counting numbers as state IDs, energies (cm^{-1}, either experimental or calculated) and their uncertainties (cm^{-1}), lifetimes (s), and standard set of quantum numbers generated by Duo. The Trans file contains state counting numbers (IDs) for upper and lower states, Einstein A coefficients (s^{-1}), and transition wavenumbers (cm^{-1}).

Table 1. Statistics on the line lists computed.

Isotopologue	No. of states	No. of transitions
^{58}NiH	11982	644490
^{60}NiH	11986	644508
^{62}NiH	11995	645386
^{58}NiD	23120	1708460

The partition functions for all four isotopologues of NiH were generated using ExoCross (Yurchenko et al. 2018b) by summing over the energy levels up to J = 60.5 (separate States files were compiled for this). The ^{58}NiH values were compared to estimates given by Sauval & Tatum (1984) as shown in Fig. 5 for temperature up to 10000 K. For this comparison, a factor of 2 was applied to the values of Sauval & Tatum (1984) to account for the nuclear spin degeneracy of ^{58}NiH. This is because ExoMol's convention is to include the nuclear spin degeneracy into ExoMol partition functions (Pavlenko et al. 2020). There is a large discrepancy between us and Sauval & Tatum (1984), with our values being significantly larger indicating possible under-count of states in Sauval & Tatum (1984), despite Sauval & Tatum (1984)'s claim that their partition function's estimate should be valid for temperatures in the range of 1000-9000 K. According to Sauval & Tatum (1984), their partition functions are based on the spectroscopic parameters from Huber & Herzberg (1979), which does not appear to cover the $W\,^2\Pi$ and $V\,^2\Sigma^+$ electronic states. As a test of the assumption that the difference is due to the lack of the $W\,^2\Pi$ and $V\,^2\Sigma^+$ energies, in Fig. 5 we show a partition function of ^{58}NiH produced using the $X\,^2\Delta$ state only (i.e. excluding $W\,^2\Pi$ and $V\,^2\Sigma^+$). This time the agreement with Sauval & Tatum (1984) is very close up to about 6000 K, which supports our assumption. We conclude that (i) the partition function of NiH by Sauval & Tatum (1984) is severally incomplete even at moderate temperatures and should not be used and (ii) our partition function should be complete at least up to 6000 K if we believe completeness of $X\,^2\Delta$ of Sauval & Tatum (1984). We note that the more recent NiH partition function of Barklem & Collet (2016) is based on use of the same data as Sauval & Tatum (1984) and gives similarly underestimated results.

The completeness of our line list is also affected by the energy threshold used (20000 cm^{-1} for the lower state), and even more so by the absence of the upper electronic states in our model. The next doublet electronic state of NiH lies at about 16600 cm^{-1} (Zou & Liu 2007), which overlaps with the energy coverage in our line list.

Figure 6 shows the comparison of partition functions for ^{58}NiH and ^{58}NiD computed with Duo and ExoCross. These partition functions were divided by the respective nuclear spin multiplicity factors (2 for ^{58}NiH and 3 for ^{58}NiD), so that the only difference between these partition functions is due to different number of states. ^{58}NiD contains more states within the same temperature range compared to ^{58}NiH, see Table 1, and thus leads to a larger value of the partition function.

We replaced calculated energy levels of ^{58}NiH, ^{60}NiH, and ^{62}NiH with the empirical ones of Havalyova et al. (2021) and the energy values of ^{58}NiD with the empirical values of Abbasi et al. (2018); Ross et al. (2019), see the `Ma/Ca` column in Table 2). Experimental

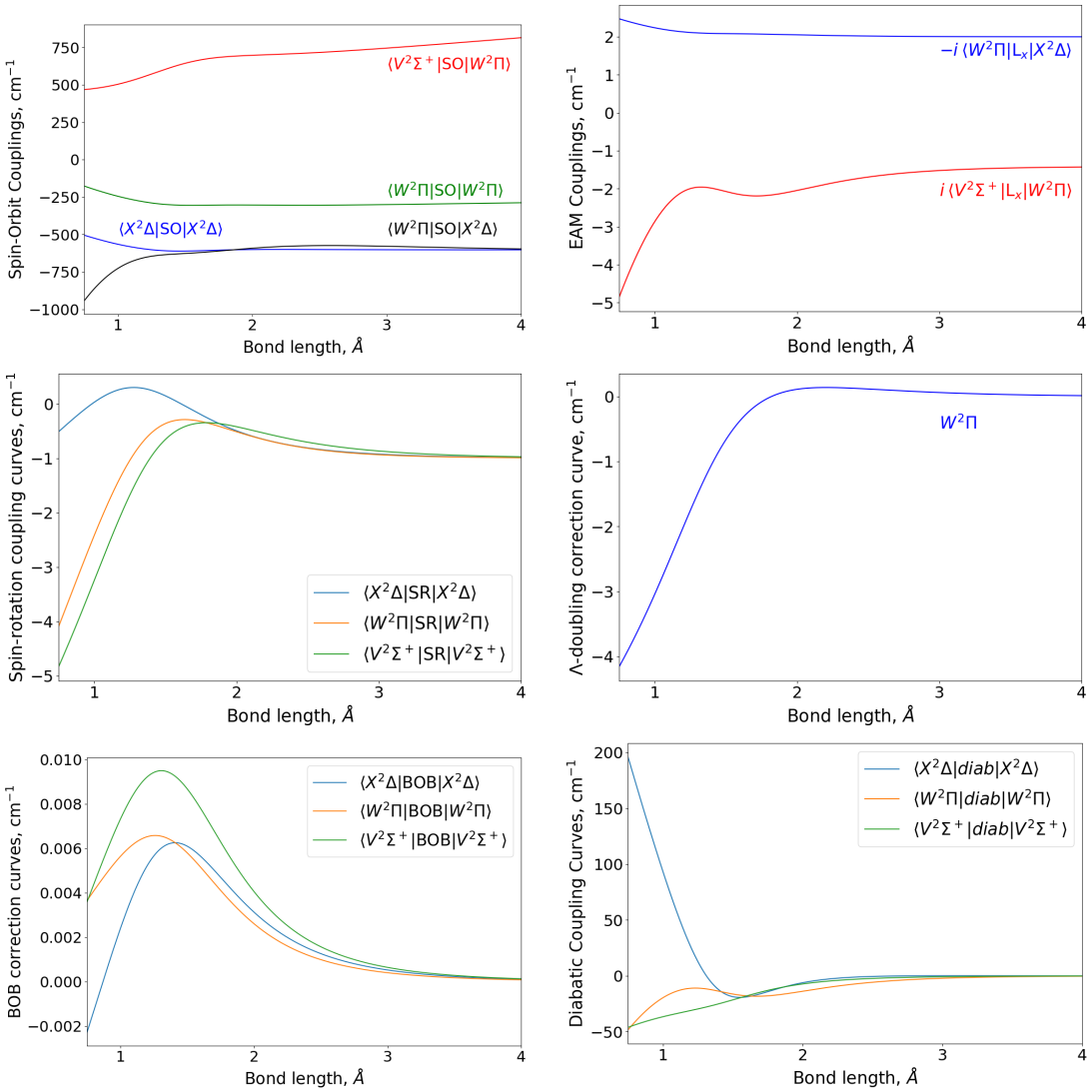

Figure 3. Empirical coupling and correction curves for ^{58}NiH and diabatic coupling curves for ^{58}NiD.

Table 2. Extract from the states file of the line list for ^{58}NiH.

i	$\tilde{E}$ (cm^{-1})	g_i	J	unc. (cm^{-1})	τ (s^{-1})	Parity	State	v	Λ	Σ	Ω	Ma/Ca	$\tilde{E}$ (cm^{-1})
1294	5689.048000	20	4.5	0.010000	1.7350E-02	+ e	V2Sigma+	2	0	0.5	0.5	Ma	5689.032591
1295	6231.011000	20	4.5	0.010000	1.3244E-02	+ e	W2Pi	2	1	0.5	1.5	Ma	6230.995724
1296	6850.718132	20	4.5	0.943406	1.4816E-02	+ e	X2Delta	3	2	-0.5	1.5	Ca	6850.718132
1297	7199.196748	20	4.5	0.597656	1.2959E-02	+ e	W2Pi	2	1	-0.5	0.5	Ca	7199.196748
1298	7364.337000	20	4.5	0.010000	1.0825E-02	+ e	X2Delta	4	2	0.5	2.5	Ma	7364.302361
1299	7370.346207	20	4.5	0.846990	1.1695E-02	+ e	V2Sigma+	3	0	0.5	0.5	Ca	7370.346207
1300	7870.980410	20	4.5	0.880736	1.0294E-02	+ e	W2Pi	3	1	0.5	1.5	Ca	7870.980410
1301	8571.359023	20	4.5	1.248474	1.1323E-02	+ e	X2Delta	4	2	-0.5	1.5	Ca	8571.359023

i: state counting number, $\tilde{E}$: state energy term values in cm^{-1}, experimental or calculated (Duo), g_i: total statistical weight, equal to $g_{\rm ns}(2J+1)$, J: total angular momentum, unc: uncertainty, cm^{-1}, τ: lifetime (s^{-1}), +/−: total parity, e/f: rotationless parity, State: electronic state, v: state vibrational quantum number, Λ: projection of the electronic angular momentum, Σ: projection of the electronic spin, Ω: projection of the total angular momentum, $\Omega = \Lambda + \Sigma$, Label: 'Ma' is for "MARVELised" and 'Ca' is for Calculated, $\tilde{E}$: State energy term values in cm^{-1}, Calculated (Duo).

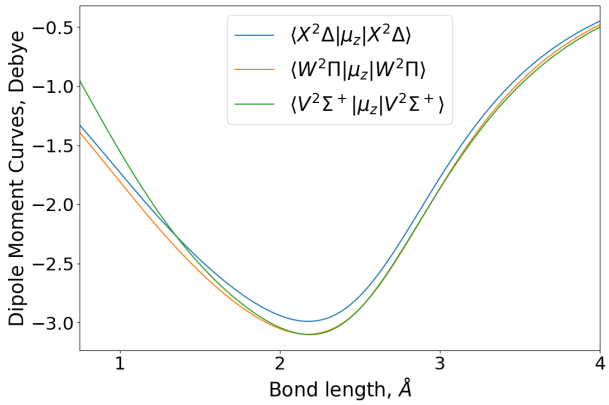

Figure 4. Diagonal dipole moments curves of NiH along the z-axis.

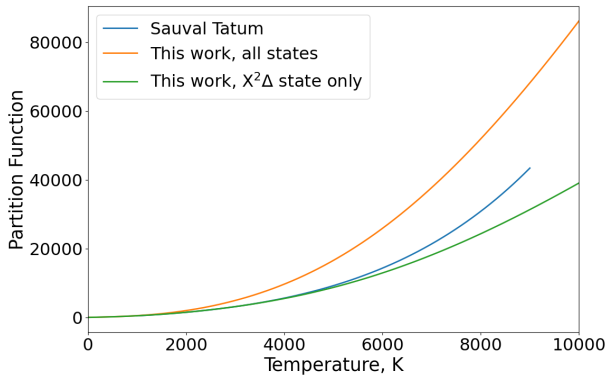

Figure 5. Our partition function of ^{58}NiH (upper curve) compared to that of Sauval & Tatum (1984) (middle curve). The lower curve is also our partition function but without the $W\,^2\Pi$ and $V\,^2\Sigma^+$ energy contributions (see text for details).

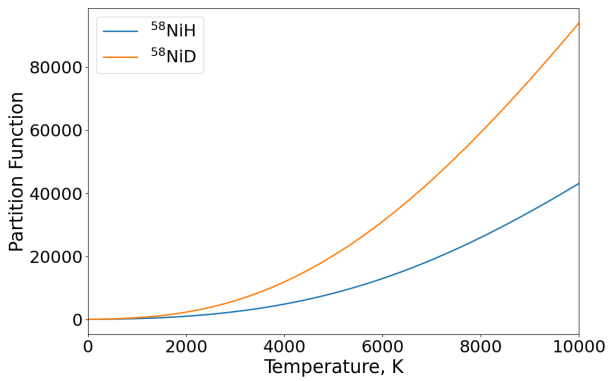

Figure 6. Comparison of our partition function of ^{58}NiD (upper curve) and ^{58}NiH (lower curve) divided by their respective nuclear spin multiplicity factors.

uncertainties for these "MARVELised" energy term values were used in the uncertainty column of the States file (see column 5 in the table 2). For calculated energy term values, we assumed uncertainties to be linearly proportional to vibrational quantum numbers ($\propto v$) and quadratic proportional rotational quantum numbers ($\propto J(J+1)$). Thus, the following equation was constructed:

$$\mathrm{unc} = av + bJ(J+1) + c, \qquad (7)$$

Table 3. Extract from the transitions file of the line list for ^{58}NiH.

f	i	A_{fi} (s^{-1})	$\tilde{\nu}_{fi}$
86	2	2.5994E+00	3507.834917
4557	4339	1.1809E-01	3507.843566
10521	10309	1.8971E+00	3507.862606
543	728	3.3705E+00	3507.902567
4936	4722	6.2377E-01	3507.927960
6952	6735	1.1753E-01	3507.942976
5538	5722	1.1704E+00	3507.943267

f: upper state counting number; i: lower state counting number; A_{fi}: Einstein-A coefficient in s^{-1}; $\tilde{\nu}_{fi}$: transition wavenumber in cm^{-1}.

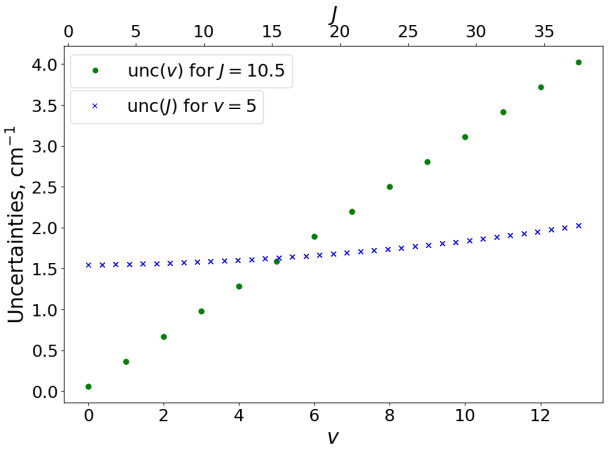

Figure 7. Uncertainties as a function of J (for fixed $v = 5$) and as a function of v (for fixed $J = 10.5$) for the $X\,^2\Delta$ state of NiH.

Table 4. Parameters for uncertainties estimation using Eq. (7).

Isotopologue and state	a	b	c
NiH, $X\,^2\Delta$	0.305	0.00033	0.020
NiH, $W\,^2\Pi$	0.283	0.00034	0.023
NiH, $V\,^2\Sigma^+$	0.275	0.00040	0.013
NiD, $X\,^2\Delta$	0.389	0.00048	0.020
NiD, $W\,^2\Pi$	0.449	0.00055	0.020
NiD, $V\,^2\Sigma^+$	0.412	0.00046	0.023

where a and b are some constants of proportionality and c is some constant offset (can be physically interpreted as a minimal possible uncertainty). These coefficients were separately identified for each electronic state. To do this, we looked at the distribution of Obs−Calc of energy term values against J and v separately. We chose the data points with the biggest Obs−Calc values and tried to adjust a, b, and c in a such way that uncertainties calculated using Eq. (7) were greater or equal than the worst Obs−Calc for corresponding J or v. Same uncertainties were used for ^{58}NiH, ^{60}NiH, and ^{62}NiH isotopologues, as they had nearly identical spectroscopic models. Uncertainties were calculated independently for ^{58}NiD isotopologue due to larger rms errors for ^{58}NiD. Table 4 gives a summary of the values of coefficients used for uncertainties calculation. Figure 7 shows examples of uncertainties as a function of J and v for the $X\,^2\Delta$ state of NiH.

4 NIH SPECTRA

Figures 8 – 11 plot four exemplary spectra of NiH. These were generated using the code ExoCross (Yurchenko et al. 2018c) with settings for a simple Gaussian line profile with HWHM = 1 cm^{-1} or HWHM = 10 cm^{-1}. Fig. 8 shows the spectra at T = 2000 K of the four isotopologues, adjusted for their abundances. Terrestrial abundances of different isotopologues of NiH were assumed to be proportional to the ratios of atomic isotopes (e.g. ^{60}NiH to ^{58}NiH ratio is the same as ^{60}Ni to ^{58}Ni). Abundances of nickel isotopes were extracted from National Nuclear Data Center (2024). Deuterium's abundance was assumed to be similar to that on Jupiter (Hersant et al. 2001).

Figure 9 shows the spectra of ^{58}NiH and ^{58}NiD not adjusted for their abundances in the shorter range of 0 – 5000 cm^{-1}. While ^{58}NiH, ^{60}NiH, and ^{62}NiH have nearly identical spectra due to a small relative change in mass of nickel atom, ^{58}NiD gives larger shifts as the relative change in mass between hydrogen and deuterium is much larger. There is a frequency shift, which is expected due to a change in mass. Moreover, there is an intensity drop, which is caused by the partition function of NiD being greater than that of NiH (as can be seen in Fig. 6).

Figure 10 shows the spectra of ^{58}NiH at different temperatures: 300 K, 1000 K, 2000 K, and 3000 K. Figure 11 shows the spectra of NiH corresponding to transitions where the upper level is specifically either in $X\,^2\Delta$ or $W\,^2\Pi$ or $V\,^2\Sigma^+$ electronic state at T = 2000 K and all of them summed up. There are no experimental or observational spectra of any of the NiH isotopologues in the range of 0–10000 cm^{-1}, so we cannot compare our generated spectra to anything. However, our spectra show the exponential decay in the intensity with the growing wavenumber, which agrees with our expectations.

Figure 12 illustrates the strongest ^{58}NiH features expected to appear in absorption from 0 to 5000 cm^{-1} at T = 1500 K. Absorptions from the lowest spin component of the ground state $X_1\,^2\Delta_{5/2}$ are most prominent. Transitions for which both the upper and lower states are based on the MARVELised (i.e. experimentally derived) values are indicated with empty symbols at the top of each stick. One can see that the line positions for the most of the strongest transitions in this region have been determined with the experimental quality characterised, either through the direct measurement or by participating as lower/upper state values. For example, several contributions seen in the first four panels (in order of increasing wavenumber) have been observed experimentally, mostly in laser magnetic resonance (LMR) experiments, with near to room-temperature sources. The first corresponds to pure rotation, recorded in the far IR by Nelis et al. (1991). The second window suggests that the strongest lines in this region would belong to the $X\,^2\Delta \rightarrow V\,^2\Sigma^+$ electronic system, but the LMR work by Lipus et al. (1992), with limited wavenumber coverage from their laser, mentioned only the spin-forbidden $X_1\,^2\Delta_{5/2} \rightarrow X_2\,^2\Delta_{3/2}$ intercombination band around 1000 cm^{-1}. The strong features in the third panel correspond to ro-vibrational transitions from v=0 of the lowest-lying states. The $X - X$ contributions were seen both in LMR Nelis et al. (1988) and as unresolved features in matrix isolation experiments (Wright et al. 1978). The $X - W$ ($X_1\,^2\Delta_{5/2} \rightarrow W_1\,^2\Pi_{3/2}$) transitions close to 2600 cm^{-1}, and the X-X ($X_1\,^2\Delta_{5/2}$ v=0 $\rightarrow X_2\,^2\Delta_{3/2}$, v=1) contributions near 3000 cm^{-1} in panel 4 were also identified in LMR experiments (Bachem et al. 1991). Although absorptions in the higher overtones and electronic bands in the last two windows have not been observed experimentally, their upper levels have been charted by optical emission spectroscopy.

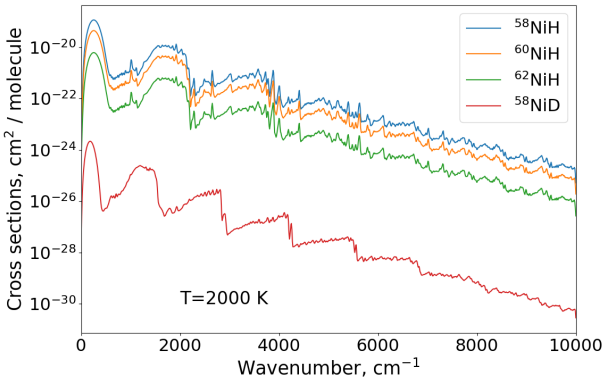

Figure 8. NiH isotopologues absorption spectrum adjusted for natural abundances generated using the Gaussian profile with HWHM = 10 cm^{-1} and T = 2000 K.

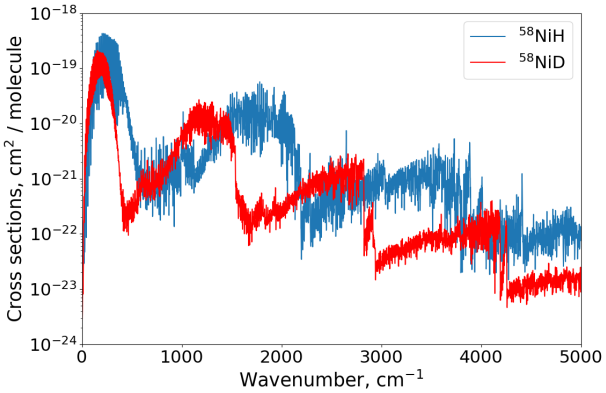

Figure 9. ^{58}NiH and ^{58}NiD absorption spectrum not adjusted for abundances generated using the Gaussian profile with HWHM = 1 cm^{-1} and T = 2000 K.

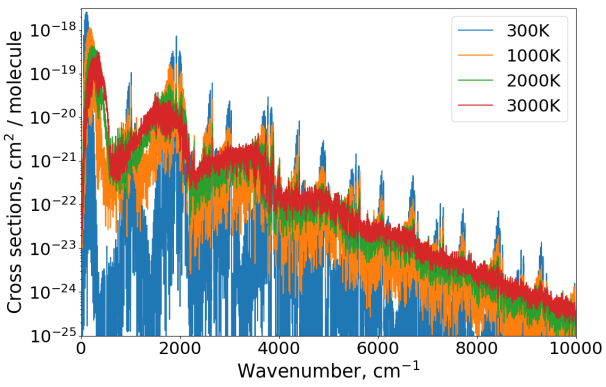

Figure 10. Temperature dependence of the ^{58}NiH absorption spectrum using the Gaussian profile with HWHM = 1 cm^{-1}.

5 CONCLUSIONS

The IR line lists BYOT for four isotopologues of NiH are provided for the first time in the range up to 10000 cm^{-1}, considering transitions and energies from the three lowest electronic states $X\,^2\Delta$, $W\,^2\Pi$ and $V\,^2\Sigma^+$. We recommend using these line lists for temperatures up to 3000 K. They are available online from www.exomol.com.

More experimental data are required to improve the precision of the spectroscopic model of the three states considered here, as we

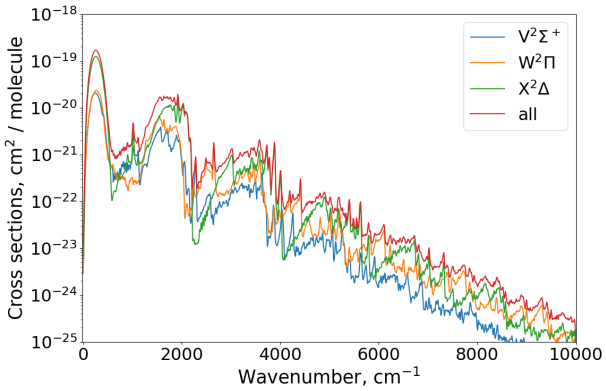

Figure 11. ^{58}NiH absorption spectrum generated using the Gaussian profile with HWHM = 10 cm^{-1} at T = 2000 K and transitions to different upper electronic states.

did not have any experimental values for levels with J higher than 16.5. More importantly, *ab initio* calculations of higher electronic states (e.g. $^2\Sigma^-$, $^4\Phi$ and others) are exceedingly required, especially considering the importance of NiH in the visible in astrophysical applications. The optical region has been studied experimentally, while the theory is far behind.

ACKNOWLEDGEMENTS

This work was supported by the European Research Council (ERC) under the European Union's Horizon 2020 research and innovation programme through Advance Grant number 883830 and the STFC Projects No. ST/Y001508/1. The authors acknowledge the use of DiRAc. KB acknowledges the support of the UCL MAPS Faculty Research Internships scheme. The authors acknowledge the use of the DiRAC Data Intensive service (CSD3) at the University of Cambridge, managed by the University of Cambridge University Information Services and the DiRAC Data Intensive service (DIaL2) at the University of Leicester, managed by the University of Leicester Research Computing Service on behalf of the STFC DiRAC HPC Facility (www.dirac.ac.uk). The DiRAC services at Cambridge and Leicester were funded by BEIS, UKRI and STFC capital funding and STFC operations grants.

DATA AVAILABILITY

The states, transition and partitions function files for NiH BYOT line lists can be downloaded from www.exomol.com. The open access programs Duo, ExoCross and pyExoCross are available from github.com/exomol.

SUPPORTING INFORMATION

Supplementary data are available at MNRAS online. This includes the spectroscopic models in the form of the Duo input file, containing all the curves, and parameters.

REFERENCES

Abbasi M., Shayesteh A., Crozet P., Ross A. J., 2018, J. Mol. Spectrosc., 349, 49
Bachem E., Urban W., Nelis T., 1991, Mol. Phys., 73, 1031
Bagus P. S., Bjorkman C., 1981, Phys. Rev. A, 23, 461
Barklem P. S., Collet R., 2016, A&A, 588, A96
Bauschlicher C. W., Langhoff S. R., Komornicki A., 1990, Theor. Chim. Acta., 77, 263
Beaton S. P., Evenson K. M., Nelis T., Brown J. M., 1988, J. Chem. Phys., 89, 4446
Blomberg M. R. A., Siegbahn P. E. M., Roos B. O., 1982, Mol. Phys., 47, 127
Brown J. M., Beaton S. P., Evenson K. M., 1993, ApJ, 414, L125
Chen J., Steimle T. C., 2008, Chem. Phys. Lett., 457, 23
Diaconu C. V., Cho A. E., Doll J. D., Freeman D. L., 2004, J. Chem. Phys., 121, 10026
Douketis C., Scoles G., Marchetti S., Zen M., Thakkar A. J., 1982, J. Chem. Phys., 76, 3057
Goel S., Masunov A. E., 2008, J. Chem. Phys., 129, 214302
Gray J. A., Rice S. F., Field R. W., 1985, J. Chem. Phys., 82, 4717
Gray J. A., Li M. G., Field R. W., 1990, J. Chem. Phys., 92, 4651
Gray J. A., Li M. G., Nelis T., Field R. W., 1991, J. Chem. Phys., 95, 7164
Guse M. P., Blint R. J., Kunz A. B., 1977, Int. J. Quantum Chem., 11, 725
Havalyova I., Bozhinova I., Pashov A., Ross A. J., Crozet P., 2021, J. Quant. Spectrosc. Radiat. Transf., 272, 107800
Hersant F., Gautier D., Huré J.-M., 2001, ApJ, 554, 391
Hill E. J., Field R. W., 1990, J. Chem. Phys., 93, 1
Huber K. P., Herzberg G., 1979, Molecular Spectra and Molecular Structure IV. Constants of Diatomic Molecules. Van Nostrand Reinhold Company, New York, doi:10.1007/978-1-4757-0961-2, https://doi.org/10.1007/978-1-4757-0961-2
Kadavathu S. A., Lofgren S., Scullman R., 1987, Physica Scripta, 35, 277
Kadavathu S. A., Scullman R., Gray J. A., Li M. G., Field R. W., 1990, J. Mol. Spectrosc., 140, 126
Le Roy R. J., 2017, J. Quant. Spectrosc. Radiat. Transf., 186, 167
Lee E. G., Seto J. Y., Hirao T., Bernath P. F., Le Roy R. J., 1999, J. Mol. Spectrosc., 194, 197
Li M. G., Field R. W., 1989, J. Chem. Phys., 90, 2967
Lipus K., Simon U., Bachem E., Nelis T., Urban W., 1989, Mol. Phys., 67, 1431
Lipus K., Bachem E., Urban W., 1992, Mol. Phys., 75, 945
Lipus K., Urban W., Evenson K. M., Brown J. M., 1993, Mol. Phys., 79, 571
Marian C. M., Blomberg M. R. A., Siegbahn P. E. M., 1989, J. Chem. Phys., 91, 3589
McCarthy M. C., Kanamori H., Steimle T. C., Li M. G., Field R. W., 1997, J. Chem. Phys., 107, 4179
Medvedev E. S., Meshkov V. V., Stolyarov A. V., Ushakov V. G., Gordon I. E., 2016, J. Mol. Spectrosc., 330, 36
National Nuclear Data Center 2024, NuDat database, www.nndc.bnl.gov/nudat/
Nelis T., Bachem E., Bohle W., Urban W., 1988, Mol. Phys., 64, 759
Nelis T., Beaton S. P., Evenson K. M., Brown J. M., 1991, J. Mol. Spectrosc., 148, 462
O'Brien L. C., O'Brien J. J., 2005, ApJ, 621, 554
Pavlenko Y. V., Yurchenko S. N., Tennyson J., 2020, A&A, 633, A52
Pouamerigo R., Merchan M., Nebotgil I., Malmqvist P. A., Roos B. O., 1994, J. Chem. Phys., 101, 4893
Prajapat L., Jagoda P., Lodi L., Gorman M. N., Yurchenko S. N., Tennyson J., 2017, MNRAS, 472, 3648
Robert J. Le Roy Carl C. Haugen J. T., Li H., 2011, Mol. Phys., 109, 435
Ross A. J., Crozet P., Richard C., Harker H., Ashworth S. H., Tokaryk D. W., 2012, Mol. Phys., 110, 2019
Ross A. J., Crozet P., Adam A. G., Tokaryk D. W., 2019, J. Mol. Spectrosc., 362, 45
Ruette F., Blyholder G., Head J., 1984, J. Chem. Phys., 80, 2042
Sauval A. J., Tatum J. B., 1984, ApJS, 56, 193
Scullman R., Lofgren S., Kadavathu S. A., 1982, Physica Scripta, 25, 295
Shaji S., Nunn J., O'Brien J. J., O'Brien L. C., 2008, ApJ, 672, 722
Shaji S., Song A., Li M., O'Brien J. J., O'Brien L. C., 2009, Can. J. Phys., 87, 583
Steimle T. C., Nachman D. F., Shirley J. E., Fletcher D. A., Brown J. M., 1990, Mol. Phys., 69, 923

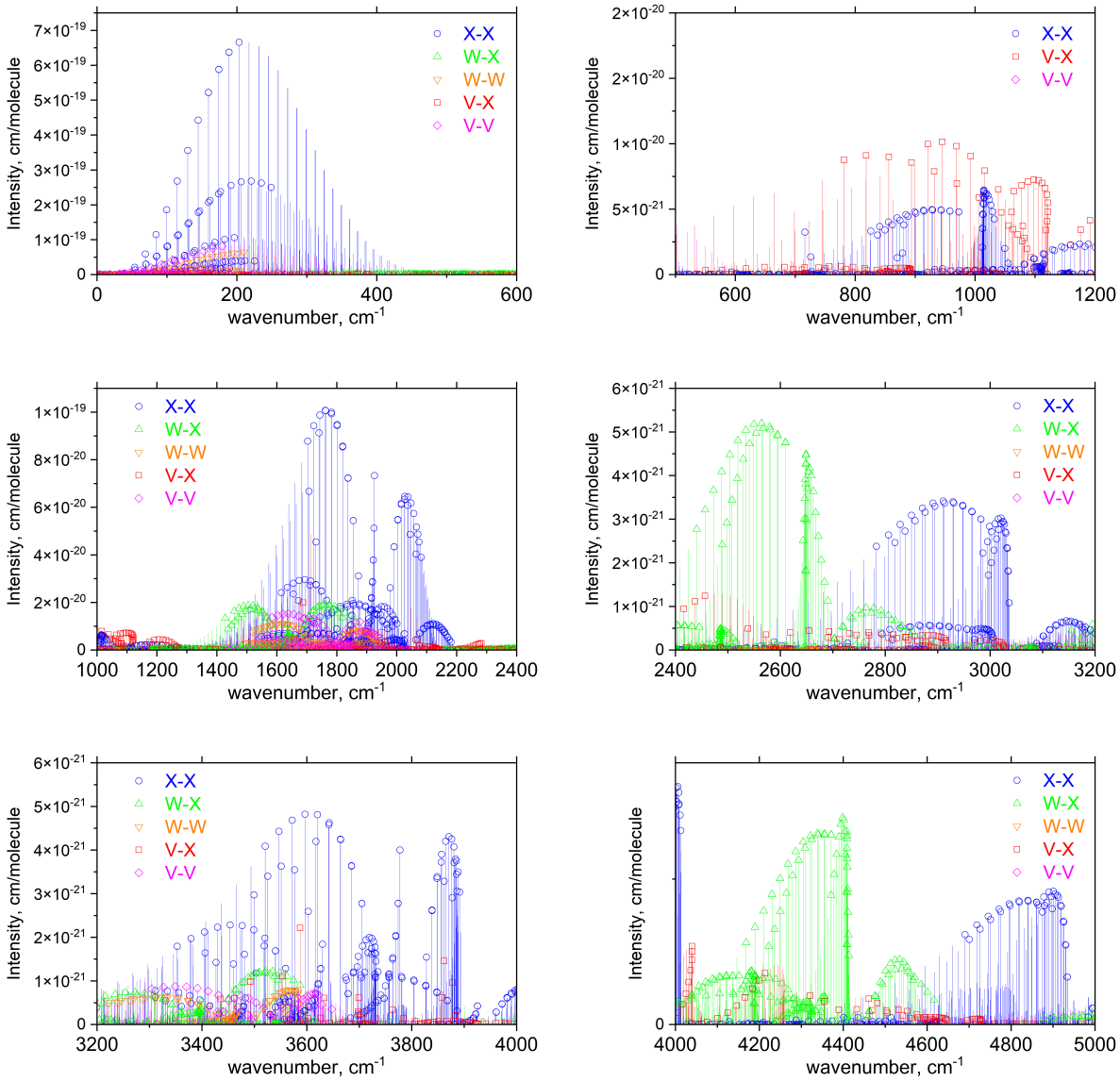

Figure 12. ^{58}NiH absorption spectra, T = 1500 K showing line intensities as heights of sticks and divided into six spectroscopic windows below 5000 cm^{-1}. Empty symbols indicate "MARVELised" transitions i.e. where both the upper and lower states energy values are experimentally derived (MARVEL).

Tennyson J., Yurchenko S. N., 2012, MNRAS, 425, 21
Tennyson J., Hill C., Yurchenko S. N., 2013, in 6th international conference on atomic and molecular data and their applications ICAMDATA-2012. AIP, New York, pp 186–195, doi:10.1063/1.4815853
Tennyson J., et al., 2020, J. Quant. Spectrosc. Radiat. Transf., 255, 107228
Tennyson J., et al., 2024, J. Quant. Spectrosc. Radiat. Transf., 326, 109083
Vallon R., Richard C., Crozet P., Wannous G., Ross A., 2009, ApJ, 696, 172
Walch S. P., Bauschlicher C. W., 1983, J. Chem. Phys., 78, 4597
Walch S. P., Bauschlicher C. W., Langhoff S. R., 1985, J. Chem. Phys., 83, 5351
Werner H.-J., Knowles P. J., Knizia G., Manby F. R., Schütz M., 2012, WIREs Comput. Mol. Sci., 2, 242
Wright R. B., Bates J. K., Gruen D. M., 1978, Inorg. Chem., 17, 2275
Yurchenko S. N., Lodi L., Tennyson J., Stolyarov A. V., 2016, Comput. Phys. Commun., 202, 262
Yurchenko S. N., Sinden F., Lodi L., Hill C., Gorman M. N., Tennyson J., 2018a, MNRAS, 473, 5324
Yurchenko S. N., Al-Refaie A. F., Tennyson J., 2018b, A&A, 614, A131
Yurchenko S. N., Al-Refaie A. F., Tennyson J., 2018c, A&A, 614, A131
Zou W., Liu W., 2007, J. Comput. Chem., 28, 2286

This paper has been typeset from a TEX/LATEX file prepared by the author.